LIGO Analogy Lab Experiments

P444 Integrated Experimental Lab II

Submitted By: Nisarg Vyas
Roll No. 1711091

School of Physical Sciences
National Institute of Science Education and Research

September 16, 2021

Aknowledgement

First and foremost thanks to Dr. Santosh Babu Gunda, Scientific Officer-E, SPS NISER. His enthusiasm for the lab is unparalleled and he shares the joys of troubleshooting with each of the lab students.
Special thanks to Dr. Ritwick Das for helping with his quick insights and interactions in the lab. Finally many due thanks to the department for providing us such an opportunity to explore physics in the lab.

Contents

Abstract

Sound waves, in analogy with the gravitational waves, are detected using interferometry. A Michelson interferometer with Fabry-Perot cavity is setup and the distances are optimised to achieve maximum sensitivity. Any disturbance then leads to a shift in fringe pattern is detected by a photo-diode and Fourier transformed to get the corresponding frequencies. At the end we discuss various observations and suggest possible reasons for them.

1 Introduction

In September 2015, almost 100 years after their prediction by Dr. Albert Einstein, the gravitational waves were first detected at the Laser Interferometer Gravitational-Wave Observatory (LIGO). These waves produce extremely tiny strains in the fabric of space time, of the order of a thousandth part of the charge radius of a proton. Such a highly sensitive detector had to develop and employ various frontier technologies to achieve this. The complexity of the set-up is therefore understandably high. In order to breakdown the detector physics to the understanding of an undergraduate student, a few authors have suggested some ways. Lior M. Burko in [3] suggests students to computationally understand and process the LIGO 2015 signal to calculate a few parameters while Mathur et al in [2] indulge students into deriving various formula and calculating parameters just with basic physics knowledge and the LIGO black hole merger data from 2015. However, Ugolini et al in [1] bring in an entirely new perspective by drawing analogy of gravitational wave detection to sound wave detection experiment, which is elegant and doable in any undergraduate lab. In the performed experiment we follow [1] to construct a sensitive sound wave detector using interferometers. A small review of the basics of interferometers used, and a quick glance at LIGO precedes our experimental details.

1.1 Michelson interferometer

The Michelson interferometer (MI) designed by Albert Abraham Michelson, uses a beam splitter to divide a light beam into two arms each having a mirror at the end to reflect these beams back on the same path. The reflected beams pass the beam splitter once again and begin moving in the same direction. Here the beams interfere to give a circular or straight fringe pattern depending on whether the mirrors (at the end of each arm) are parallel or not. The schematic design is shown in the figure 1.1.

It should be easy to deduce that if the arm lengths are d_1 and d_2 (say, $d_2 > d_1$), then twice their difference $2d = 2(d_2 - d_1)$ is the extra distance traversed by the light beam going to mirror 2 (shown in red in figure 1.1). Had the incident light rays made an angle θ with the normal to the mirror, the path difference would be $2dcos\theta$. Also, the one that moves to mirror 1, passes through the beam splitter (refractive index, say μ) thrice while the other one passes through it only once. Therefore an extra path difference of $2(\mu - 1)t$ is introduced. Thus the path difference between the interfering beams is:

$$\Delta = 2dcos\theta - 2(\mu - 1)t$$

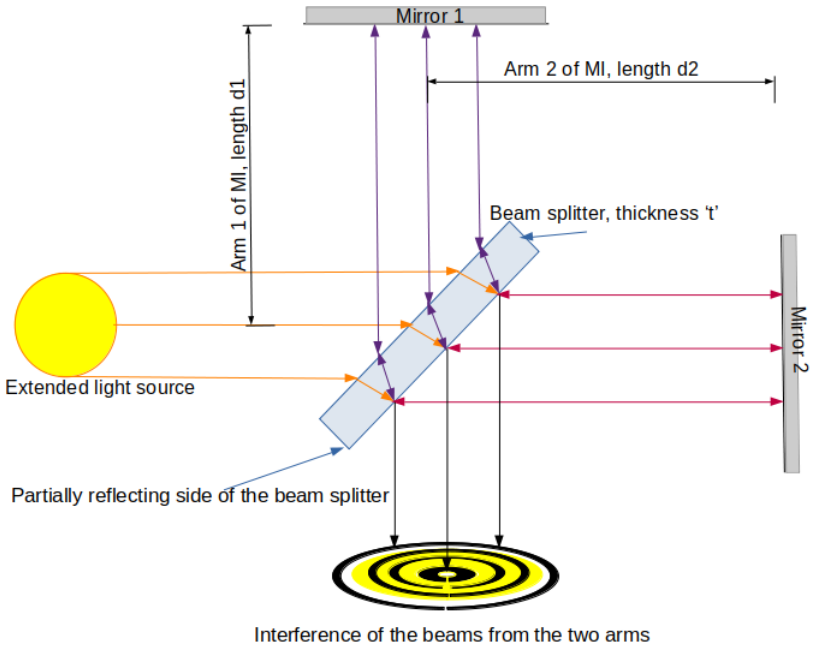

Figure 1.1: Schematic diagram of a Michelson interferometer.

The path difference arising due to the beam splitter can be compensated in the other beam by introducing a compensation plate of same refractive index and thickness. For a given set-up, the $2(\mu - 1)t$ term is constant and only the path difference resulting from difference in arm lengths is made dynamic by putting the mirrors on a translational

stage. Therefore generally, the optical path difference and hence the interference conditions for MI is given as:

$$\Delta = 2d\theta = \begin{cases} n\lambda & \text{constrtuctive interference} \\ (2n+1)\frac{\lambda}{2} & \text{destructive interference} \end{cases} \tag{1.1}$$

For a given n, d and λ, θ is constant and therefore the locus of bright or dark fringe becomes a circular ring.

1.2 Fabry-Perot cavity

Fabry-Perot interferometer consists of two parallel mirrors one of which reflects only partially (e.g. a beam splitter) thus creating a multitude of reflections between the two mirrors. Various orders of reflected beams come out of this optical cavity (OC) formed between the two mirrors, to interfere and produce circular fringes. The working of a Fabry-Perot cavity is explained in the diagrams and the derivation with follows. Let the partial reflecting mirror have

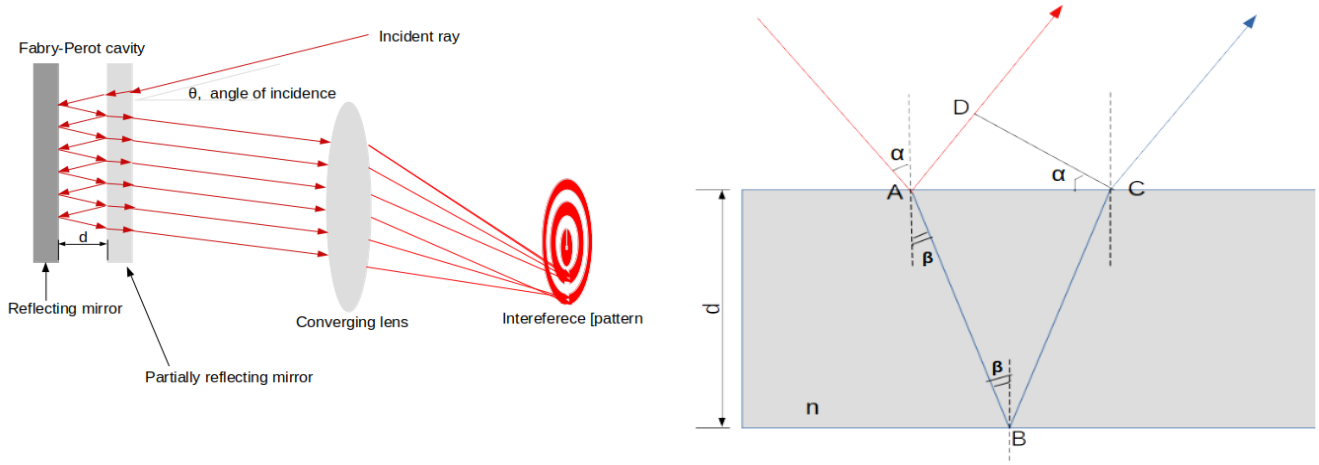

(a) (b)

Figure 1.2: Working of a Fabry-Perot cavity

a refractive index 'n', the optical path difference between two consecutive reflections from the cavity can be given as (see figure 1.2b):

$$\Delta = n(AB + BC) - AD$$

AD can be written as: $ACsin\alpha$, but $AC = 2dtan\beta$ and using Snell's law, $sin\alpha = nsin\beta$, therefore, $AD = (2dtan\beta)nsin\beta$ and $AB = d/cos\beta$ Substituting the above terms, one gets

$$\Delta = 2ndcos\beta$$

Note that any two consecutive reflections will have the same optical path difference, and the corresponding phase difference will be:

$$\delta = \frac{2\pi}{\lambda}\Delta$$

The output intensity at any m^{th} reflection can be calculated with:

$$I = I_0 \frac{1}{1 + Fsin^2(\delta/2)}$$

where finesse, $F = \frac{4R}{(1-R)^2}$ if the mirrors forming the cavity have reflectivity 'R'. If the reflectivity of the two mirrors differ (say, R_1, R_2) then the finesse is given as:

$$F = \frac{\pi(R_1R_2)^{\frac{1}{4}}}{1 - (R_1R_2)^{\frac{1}{2}}} \tag{1.2}$$

In the context of the experiment at hand, note that the multiple reflections of the optical cavity increase the sensitivity of the set-up to the changes in the cavity length. That is if the first reflection and interfered with the m^{th} reflection, and the cavity as disturbed by Δd then the total path difference in the two beams is $m \times (2n\Delta dcos\beta)$.

1.3 LIGO

The Laser Interferometer Gravitational-wave Observatory (LIGO) seeks to detect gravitational waves by measuring the strain in the space-time produced by them, using laser interferometry. The setup consists of a Michelson interferometer of arm length 4 km. Each of the arm is folded about 450 times to increase the sensitivity. Needless to say, this requires a very high finesse Fabry-Perot cavity which is achieved with high reflectivity mirrors, vacuum operation of all the optical parts and by operating the interferometer at large laser power.

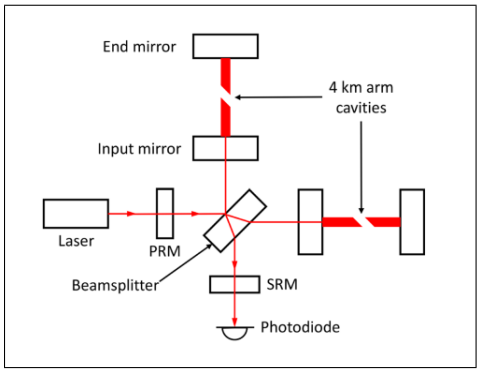

Figure 1.3: Schematic diagram of the set-up used in advance LIGO

Arm length of 4 km, folding the arms by using optical cavities, and using solid state Nd-YAG laser ($\lambda = 1064nm$) gives a strain sensitivity of:

$$h = \frac{\delta L}{L} = \frac{1064 \times 10^{-9}}{450(4 \times 10^3)} \approx 10^{-13}$$

However this is not enough since the theory of general relativity predicts a strain of 10^{-21} or lower would be needed to resolve the gravitational waves. The rest of the strain sensitivity is increased by "splitting" the fringes into a gradation from dark to bright. This is done through beam modulation, using sensitive detectors and by operating near the dark fringe.
In order deploy above techniques to achieve high strain sensitivity, the interferometer needs to operate at high laser power ($\sim 750kW$) while the input laser can provide only about $40W$. The power recycling mirrors (PRM) and the signal recycling mirrors (SRM) push the laser power back into the set-up to achieve high operating laser power.

2 The analogy experiments

As we have seen, the LIGO set-up uses a Michelson interferometer with an optical cavity in both the arms which provides very high sensitivity. Each folding of the arm of an MI provides increased sensitivity, but also requires precise alignments, thus there is a trade-off between precise alignment and sensitivity. We deploy this idea in our set-up by using an MI with an optical cavity in only one of the arms (**??**).
The set-up (**??**) consists of (1) a HeNe laser, (2) a beam splitter (70:30), (3) another beam splitter (50:50), (4) first mirror of MI, (5) second mirror of MI. and (6) a photo-diode. The notation for beam splitters is such that the numbers before and after the colon indicate the amount of light intensity they reflect and transmit. In that notation, eg. the 70:30 beam splitter (2) reflects 70% of the light while transmitting the rest. This component

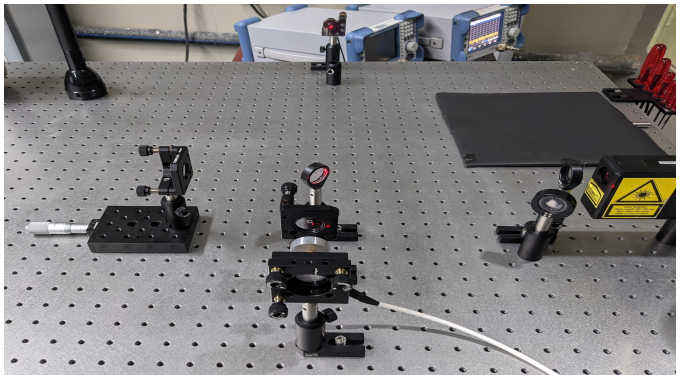

Figure 2.1: The laboratory set-up

is so arranged that the majority of light goes into the optical cavity arm wherein, due to multiple reflections, the beam suffers most reduction in intensity. This is done to make sure that when the two beams from the two MI arms interfere at the photo-diode, there isn't much difference in there intensities. We first performed the exercise of aligning the interferometer and the cavity, without (6). The interference patter was projected onto a distant screen and observed (**??**).

The laser (1) was aligned onto the centre of beam splitter (2) which was placed at 45° with respect to the incident laser beam coming from the beam expander (7). Without (3) in place, the laser beam was aligned to fall at the centres of the MI mirrors (4) and (5), and adjusted to produce interference patter as shown in 2.3a. Blocking the second arm (the one without the optical cavity), the beam splitter (3) was put in place and adjusted till the planes of (3) and (4) become parallel and produce interference as shown in 2.3b. Then, the second arm was unblocked and the interference as shown in 2.3c was obtained.
Finally, the beam splitter (3) was made unparallel to MI mirror (4), this gives multiple reflections from the OC which when aligned with the reflection from the second arm of MI, produces fringes. The schematic **??** shows the first reflection of OC superimposed on that from the mirror (5), producing nice circular fringes. Note that each round trip of laser beam inside the Fabry-Perot cavity results in successively dimmer spots. In principle, the reflection from the second arm can be aligned with anyone of these, and in fact, more the round trips a beam has gone, more the sensitivity of the interference pattern formed by it. However, dimmer spots don't give a good interference pattern and thus for the rest of the experiment, we used the second reflection from the OC to interfere with that from the second arm (5).

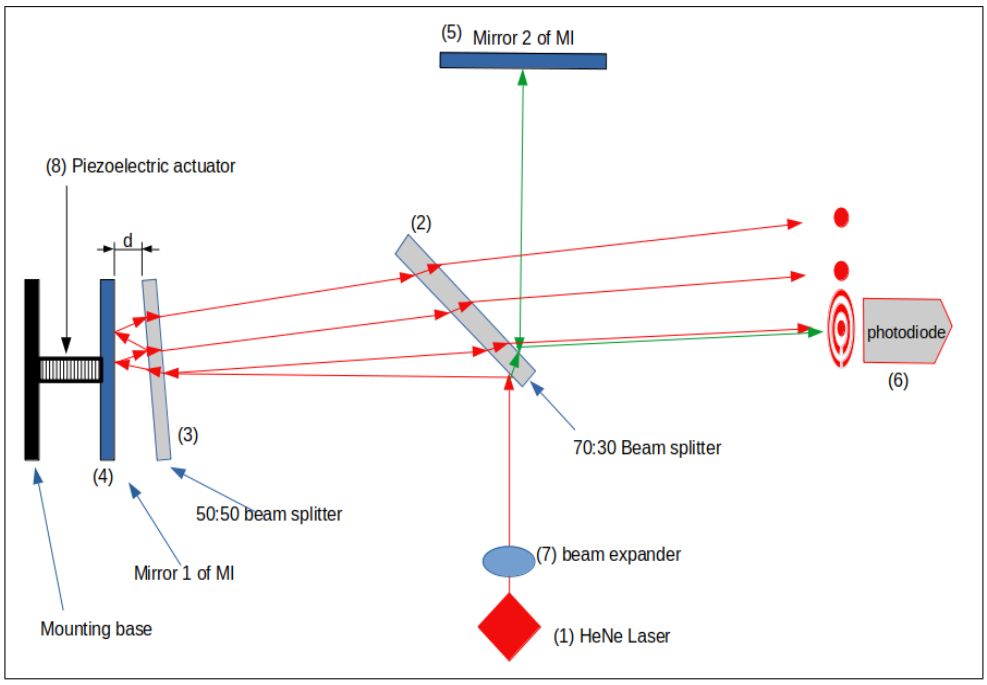

Figure 2.2: Schematic of the set-up.

(a) (b) (c)

Figure 2.3: The various interference patter as described in section (2)

Using the formula 1.2, we calculated the finesse of our optical cavity to be 7.2. Note that this is too low but good

enough for lab experiments. Contrast the value with the LIGO set-up where in the most sensitive region, the finesse is as high as 450.

2.1 Driven oscillations with piezo actuator

So far, the interference pattern was observed to be sensitive to large mechanical disturbances. For example a small punch on the optical bread board resulted in the circular fringes to move in and move of the center. But loud noises could not produce significant changes in the fringes. Since our aim is detection of sound waves, we required more sensitivity. To achieve this we tried to optimise the arm lengths of the MI. The MI mirror (5) was put on a translation stage of least count $10\mu m$. The MI mirror (4) was mounted on a piezoelectric actuator (see component list and appendix for notes on usage) and the distances of the two arms made roughly equal to proceed with the rest of the optimisation.
The laser was turned on, interference created between the second arm of MI and the second reflection from the delay line arm, was given as an input to the photo-diode. The delay line arm was then oscillated back and forth (with amplitude of a few μm) by driving the piezoelectric device with a triangular wave of frequency of few hundred Hz. The fast Fourier transform (FFT) of the photo-diode signal was continuously assessed with a spectrum analyser. The 2.4 shows output of the photo-diode when the piezo actuator is driven with a frequency of a few mHz. Note that the output shows that the set-up is least sensitive to arm-length changes at point (1) and (3) while it is the most sensitive at point (2) because of the slope of the tangents at these points. We fixed the DC offset to a level that would correspond to the point(2) and gave higher frequencies (hundreds of Hz) to the piezo for the next part in optimisation. The MI mirror (5) put on a translational stage was then moved in the both the directions for several hundred μm and an optimal point was found by hit and trial. For this part we looked at the FFT of the photo-diode output using a spectrum analyser. For different arm length differences, we obtained different heights corresponding to the same frequency peak in the FFT. The length of translational stage was fixed to that point where we got the best peak. The piezo DC offset was reset for this new arm length difference and these settings were kept constant throughout the rest of the experiment.

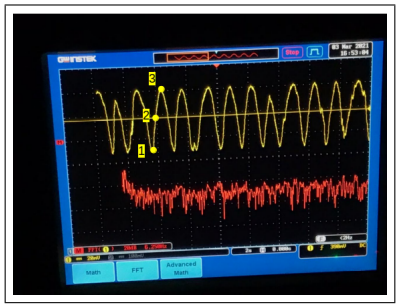

Figure 2.4: Piezo driven mirror produces a fluctuating fringe pattern which gives sinusoidal output voltage when incident on a photo-diode.

Table 2.1: Calculations for mirror driven by piezo actuator at 4 different frequencies.

Driving frequency, f_O	Detected frequency, f_D	Signal peak (dB)	Average noise level (dB)	$\Delta\ f$	Error in frequency detection (%)	SNR_{dB}
800	812.7	-71.4	-105	12.7	1.59	33.6
1200	1212.7	-64.8	-105	12.7	1.06	40.2
1400	1412.7	-58.4	-105	12.7	0.91	46.6
1600	1612.7	-59.4	-105	12.7	0.79	45.6

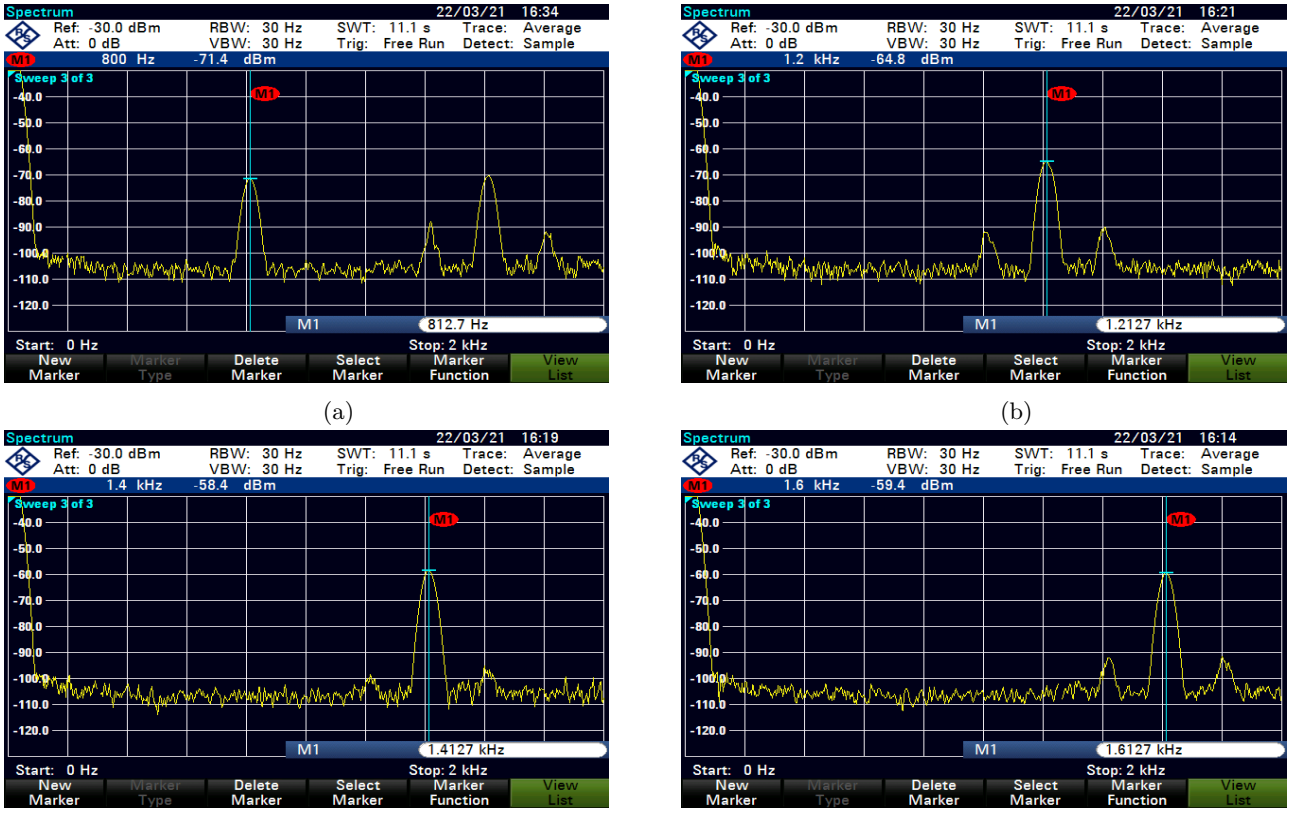

Figure 2.5: The FFT of photodiode output for different piezo driving frequencies.

2.2 Experiments with sound

Having optimised the arm lengths to achieve greatest sensitivity possible with the current set up, we gave constant frequency sound signals through a loudspeaker and recorded the corresponding FFT of the photo-diode output. It was seen that the smaller peaks observed near the expected ones (as seen in piezo driven mirrors) were now absent. Also note that the 500 Hz input shows harmonics too. These aspects are discussed in the results and discussions section.

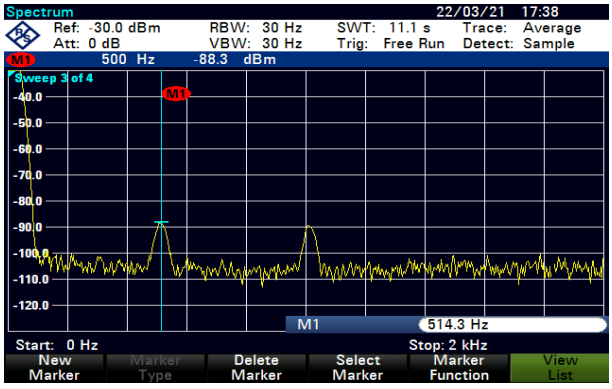

(a)

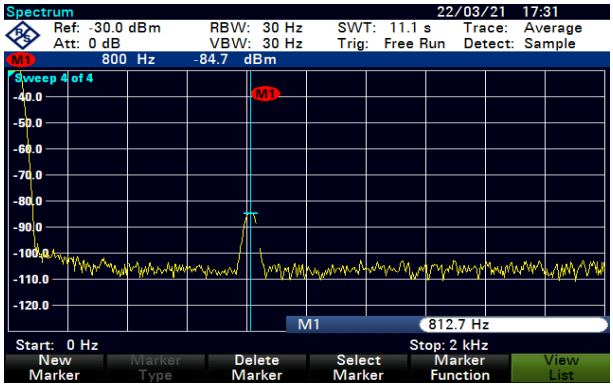

(b)

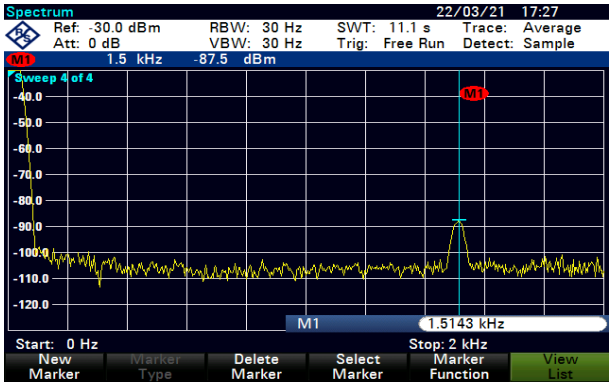

(c)

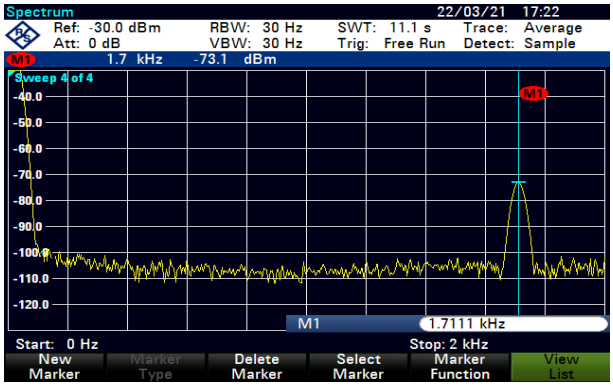

(d)

Figure 2.6: The FFT of photo-diode output for different frequencies from the speaker.

The results are summarised in the following table.

Table 2.2

Driving frequency, f_O	Detected frequency, f_D	Signal peak (dB)	Average noise level (dB)	Δf	Error in frequency detection (%)	SNR_{dB}
500	514.3	-88.3	-105	14.3	2.86	16.7
800	812.7	-84.7	-105	12.7	1.59	20.3
1500	1514.3	-87.5	-105	14.3	0.95	17.5
1700	1711.1	-73.1	-105	11.1	0.65	31.9

3 Results and discussions

On signal to noise ratio It can be seen from table 2.1 that the frequencies the driving piezo actuator can be detected at the photo-diode with an average error of $\sim 1\%$, and with an average signal to noise ratio of 41.5 dB. However, the detection of sound waves directly from the speaker has a relatively larger error in detection of input frequency, *viz-a-viz* $\sim 1.5\%$ (averaged over the frequencies used). The signal to noise ratio (SNR) for speaker input is also much lower, averaging to 21.6 dB. It should be noted from the the table 2.2 that the signal to noise ratio improved when the speaker was given higher frequencies inputs. To rule out the possibility of the speaker itself leading to such trends, we analysed the speaker output for the frequency range used in the experiment. It can be seen in figure 3.2a that the speaker emits sound in frequency range 500 Hz to 2000 Hz at almost uniform volume.

On the appearance of smaller side peaks in FFT of piezo driven mirror output It can be seen in the figures **??** that two smaller peaks of frequencies $\pm 200Hz$ arise with the central peak corresponding to the piezo output frequency. Note that these are absent from the corresponding speaker output. Also note that frequencies $200Hz$ above and below the actual input appears consistently in all of the outputs. Hence we concluded that these must be arising from poor contact between the piezo actuator and the mirror holder.

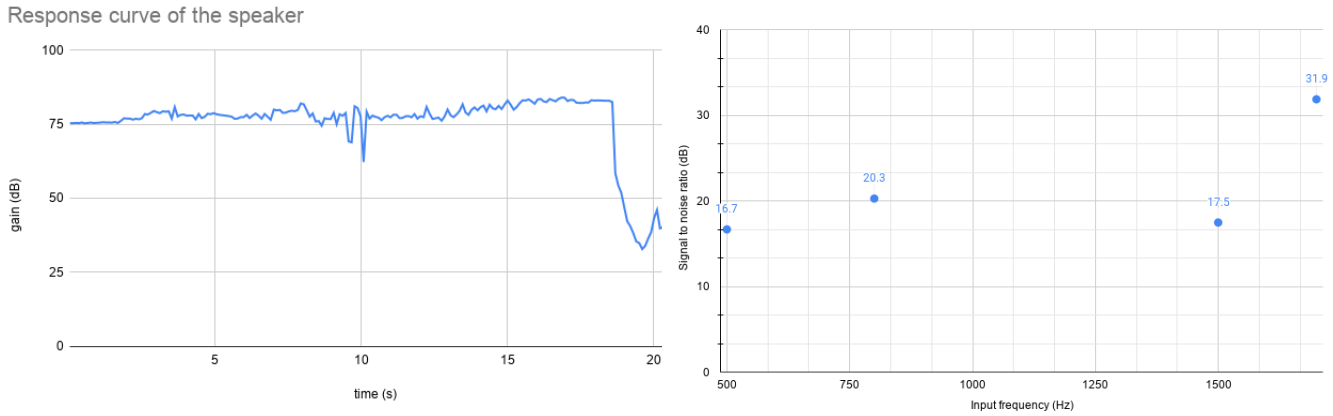

(a) Frequency response curve of the speaker.

(b) Trend of SNR with frequency

On the appearance of harmonics in fourier spectrum The figures 2.6a shows an FFT peak at 1000 Hz besides the expected one at 500 Hz. It was seen during the experiment that nearly every input frequency (upto 2 kHz) showed one or two harmonics. Those for higher frequencies aren't shown in the figures 2.6 because the frequency sweep ends at 2 kHz. However, it was also seen that lower frequencies produced many more harmonics. For example, 200 Hz produced prominent FFT peaks at all multiples upto 2 kHz (and further too, but we restricted the sweep to 2kHz due to time constraints. We proposed two plausible explanations for this. (1) The echo in the room might be

contributing to give harmonics. (2) The speaker output might itself be emitting multiple superimposed harmonic frequencies instead of the single pure harmonic it is supposed to.
To explore the matter further, we saw the FFT of the speaker sound at input frequency 500 Hz, both inside the lab and outside in open. The figures summarise the outcome.

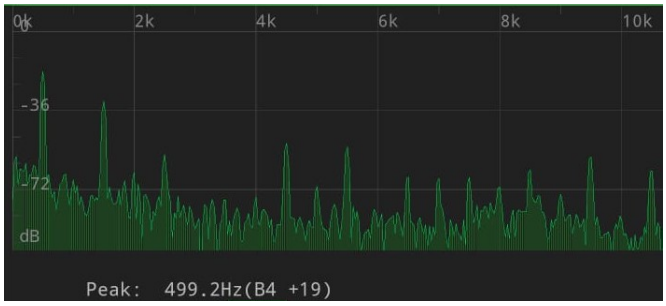

(a) Speaker output at 500 Hz. Outdoors.

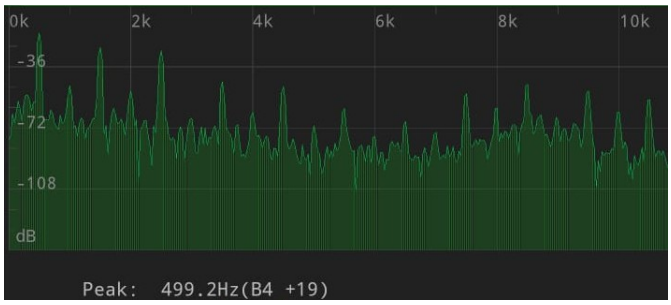

(b) Speaker output at 500 Hz. Indoors.

Figure 3.2: Notice the appearance of odd harmonics when the speaker is indoors

The above observation clearly means that the reason for appearance of harmonics is primarily due to the speaker output which is not a pure frequency as it should be, but a superposition of harmonics too. However the appearance of odd harmonics in the indoor FFT spectrum tells us that the reverberation of sound does indeed have some effect. Recall that the harmonics were observed to be more prominent and numerous for smaller frequencies, this can be explained as follows. Smaller frequencies means larger wavelength of sound waves; it is intuitive then, that it is easier to accidentally form standing waves for waves of larger wavelength. Even if standing waves aren't formed, it is easier for higher frequencies (smaller wavelength waves) to get absorbed and damped by obstructions in a laboratory, while longer wavelengths might reverberate for longer and easily.

4 Conclusion

The sensitivity of the set-up can be quantified by strain sensitivity and the signal to noise ratio. The SNRs for several input frequencies and for different sources of vibrations (piezo and speaker) were already tabulated. The actual strain sensitivity cannot be calculated due to various complex couplings between the mirror and the peizo and the holders. However, we can estimate the strain sensitivity achievable with the current optical set-up as done in section 1.3 (not including the sensitivity due to the photo-diode). This calculation ($\lambda = 632nm$) and arm lengths of about 12.5 cm yields a sensitivity of $\approx 5 \times 10^{-6}$. As the set-up successfully detected the sound waves, we infer that this sensitivity is enough for such experiments. However, it should be emphasised that the actual sensitivity might be even less, due to damping at various couplings.
Towards the end, we can conclude that the experiment's goal to detect sound waves was achieved within the given time limit. Several loose ends in the experiment can be explored further and the detection improved by optical and electronic means. One possibility is to design a negative feedback circuit which will negate the low frequency noises, thereby increasing the sensitivity in that region. Better optical components with longer arm lengths are the obvious extensions but we don't think it is needed primarily because the currently achievable (ideal) strain sensitivity (as calculated above) should be sufficient for sound detection.

Appendix

Component List

Table 4.1: List of components used.

Serial No.	Equipment	Code	Quantity
Basic components			
1	He-Ne Laser 0.8 mW	HNLS008R-EC	1
2	Photo-diode	SM05PD1A	1
3	Converging lens	LA1509	1
4	Mirror	ME1-GO1	2
5	50:50 beam splitter	EBS1	1
6	70:30 beam splitter	BST10	1
7	PZT	PK2FQP2	1
8	Lens mount	LMR1	2
9	Optical post	TR2	10
10	Post holder	PH2	10
11	Mounting base	BA2	10
12	Mirror mount	KM100T	4
Components for sound experiments			
13	USB oscilloscope	T3DSO1104	1
14	Spectrum analyser	R&S FSC3	1
15	Function generator	sndab	1
16	Loudspeaker	LiveTech Yoga speaker	1

Bibliography

[1] ""American Journal of Physics 87, 44 (2019); https://doi.org/10.1119/1.5066567

[2] "An analysis of the LIGO discovery based on introductory physics", Mathur et al, American Journal of Physics 85, 676 (2017); https://doi.org/10.1119/1.4985727

[3] "Gravitational Wave Detection in the Introductory Lab", Lior M. Burko, Phys. Teach. 55, 288 (2017); https://doi.org/10.1119/1.4981036